Water Research 103 (2016) 101–108

Contents lists available at ScienceDirect

Water Research

journal homepage: www.elsevier.com/locate/watres

The oxidation capacity of Mn_3O_4 nanoparticles is significantly enhanced by anchoring them onto reduced graphene oxide to facilitate regeneration of surface-associated Mn(III)

Lin Duan [a], Zhongyuan Wang [a], Yan Hou [a], Zepeng Wang [a], Guandao Gao [a], Wei Chen [a, **], Pedro J.J. Alvarez [b, *]

[a] College of Environmental Science and Engineering, Ministry of Education Key Laboratory of Pollution Processes and Environmental Criteria, Tianjin Key Laboratory of Environmental Remediation and Pollution Control, Nankai University, Wei Jin Road 94, Tianjin, 300071, China
[b] Department of Civil and Environmental Engineering, Rice University, Houston, TX, 77005, United States

ARTICLE INFO

Article history:
Received 11 May 2016
Received in revised form
27 June 2016
Accepted 10 July 2016
Available online 11 July 2016

Keywords:
Mn_3O_4–rGO nanocomposites
Oxidation capacity
Graphene
1-Naphthylamine

ABSTRACT

Metal oxides are often anchored to graphene materials to achieve greater contaminant removal efficiency. To date, the enhanced performance has mainly been attributed to the role of graphene materials as a conductor for electron transfer. Herein, we report a new mechanism via which graphene materials enhance oxidation of organic contaminants by metal oxides. Specifically, Mn_3O_4–rGO nanocomposites (Mn_3O_4 nanoparticles anchored to reduced graphene oxide (rGO) nanosheets) enhanced oxidation of 1-naphthylamine (used here as a reaction probe) compared to bare Mn_3O_4. Spectroscopic analyses (X-ray photoelectron spectroscopy and Fourier transform infrared spectroscopy) show that the rGO component of Mn_3O_4–rGO was further reduced during the oxidation of 1-naphthylamine, although rGO reduction was not the result of direct interaction with 1-naphthylamine. We postulate that rGO improved the oxidation efficiency of anchored Mn_3O_4 by re-oxidizing Mn(II) formed from the reaction between Mn_3O_4 and 1-naphthylamine, thereby regenerating the surface-associated oxidant Mn(III). The proposed role of rGO was verified by separate experiments demonstrating its ability to oxidize dissolved Mn(II) to Mn(III), which subsequently can oxidize 1-naphthylamine. The role of dissolved oxygen in re-oxidizing Mn(II) was ruled out by anoxic (N_2-purged) control experiments showing similar results as O_2-sparged tests. Opposite pH effects on the oxidation efficiency of Mn_3O_4–rGO versus bare Mn_3O_4 were also observed, corroborating the proposed mechanism because higher pH facilitates oxidation of surface-associated Mn(II) even though it lowers the oxidation potential of Mn_3O_4. Overall, these findings may guide the development of novel metal oxide–graphene nanocomposites for contaminant removal.

1. Introduction

Graphene-based nanocomposites are a new class of nanomaterials with great potential for removing water and wastewater pollutants (Chandra et al., 2010; Chang and Wu, 2013; Kemp et al., 2013; Lowry et al., 2012; Shen et al., 2015; Wan et al., 2012). A variety of metal oxide nanoparticles, including TiO_2, MnO_x, SnO_2, Cu_2O, and FeO_x, can be anchored to graphene materials, to develop effective sorbents or catalysts (Chen et al., 2012a; Georgakilas et al., 2012; Shen et al., 2015). These graphene-based nanocomposites often exhibit enhanced sorptive, catalytic or photocatalytic performance, compared with the respective bare metal oxide nanoparticles (Chandra et al., 2010; Fu et al., 2014; Leary and Westwood, 2011; Shen et al., 2015; Xu et al., 2015; Zhang et al., 2010). For example, a TiO_2–graphene nanocomposite was reported to exhibit much higher photocatalytic activity and stability in the degradation of benzene than bare TiO_2 (Zhang et al., 2010). Recently, it was reported that a MnO_x–graphene nanocomposite achieved over 90% removal of elemental Hg in flue gas, compared with a 50% removal by bare MnO_x (Xu et al., 2015).

A number of studies have been devoted to understand the mechanisms via which graphene oxide (GO) or reduced GO (rGO) enhances the performance of graphene-based nanocomposites in

* Corresponding author.
** Corresponding author.
E-mail addresses: chenwei@nankai.edu.cn (W. Chen), alvarez@rice.edu (P.J.J. Alvarez).

http://dx.doi.org/10.1016/j.watres.2016.07.023
0043-1354/

contaminant removal (Appavoo et al., 2014; Chandra et al., 2010; Fu et al., 2014; Gupta et al., 2014; Leary and Westwood, 2011; Li et al., 2015; Lindfors et al., 2013; Liu et al., 2016; Pastrana-Martínez et al., 2015; Shen et al., 2015; Upadhyay et al., 2014; Wang et al., 2016; Xu et al., 2015; Yao et al., 2013; Zhang et al., 2010). The commonly accepted mechanisms include: a) graphene sheets can restrain aggregation of metal oxides, rendering better dispersion and thus, larger effective surface areas of the anchored metal oxide (Appavoo et al., 2014; Chandra et al., 2010; Fu et al., 2014; Gupta et al., 2014; Li et al., 2015; Liu et al., 2016; Shen et al., 2015; Upadhyay et al., 2014; Wang et al., 2016; Yao et al., 2013); b) graphene materials can enhance the adsorption of organic pollutants to the catalysts (Fu et al., 2014; Leary and Westwood, 2011; Li et al., 2015; Liu et al., 2016; Pastrana-Martínez et al., 2015; Shen et al., 2015; Upadhyay et al., 2014; Xu et al., 2015; Zhang et al., 2010); and perhaps most importantly, c) graphene materials serve as a conductor for the electron transfer during the transformation of contaminants (Appavoo et al., 2014; Gupta et al., 2014; Leary and Westwood, 2011; Lindfors et al., 2013; Shen et al., 2015; Upadhyay et al., 2014; Xu et al., 2015; Yao et al., 2013; Zhang et al., 2010). It is important to note that GO contains abundant surface O-functional groups that are redox active; even rGO may contain substantial amounts of epoxy, phenolic, carbonyl, and carboxyl groups (Chen et al., 2012a; Georgakilas et al., 2012; Krishnamoorthy et al., 2013; Pei and Cheng, 2012). These surface O-functionalities may participate directly in redox reactions (Dreyer et al., 2010; Fan et al., 2010; Han et al., 2014; Jia et al., 2011; Pyun, 2011; Su and Loh, 2012; Sun et al., 2012). For instance, GO can effectively oxidize alcohols, and these reactions can take place under anaerobic conditions (Dreyer et al., 2010). Moreover, GO can easily react with metal ions and metal oxides (Fan et al., 2010; Han et al., 2014; Pei and Cheng, 2012). Thus, we hypothesize that when incorporated with metal oxide nanomaterials, GO/rGO may also participate in the oxidation reactions of organic contaminants as an oxidant, either by reacting directly with organic molecules or by affecting the redox states of metal oxides. Consequently, certain synergistic effects may be achieved when using GO/rGO to improve the oxidation efficiency of metal oxide nanomaterials. To date, this potentially important role of GO/rGO has not been directly investigated.

This study addresses the role(s) of graphene materials in the oxidative reactions of environmental contaminants by metal oxide–graphene nanocomposites. The oxidative transformation of 1-naphthylamine by Mn_3O_4–rGO nanocomposites was selected as the test reaction, because the reaction mechanisms of 1-naphthylamine by MnO_x have been well studied (Laha and Luthy, 1990; Li and Lee, 1999; Li et al., 2003), making 1-naphthylamine a convenient reaction probe. Moreover, 1-naphthylamine is widely used as an intermediate in the synthesis of dyes, antioxidants, herbicides, and drugs, and is frequently detected in the environment (Li and Lee, 1999; Li et al., 2003). The role of rGO in the oxidative transformation of 1-naphthylamine by Mn_3O_4–rGO nanocomposites was analyzed based on reaction kinetics comparisons with bare Mn_3O_4, and various spectroscopic analyses. Supplementary experiments that examine the oxidation of 1-naphthylamine in systems containing Mn(II) and different rGO materials, as well as effects of dissolved O_2 and pH on reaction kinetics were conducted to further understand the mechanistic role of rGO in the transformation of 1-naphthylamine by Mn_3O_4–rGO nanocomposites.

2. Materials and methods

2.1. Materials

Graphene oxide was synthesized using graphite powder (Sigma–Aldrich, U.S.) using a modified Hummers method (Zhang et al., 2015). Three Mn_3O_4–rGO composites containing different mass of Mn_3O_4 were synthesized by modifying methods reported in the literature (Li et al., 2013; Nam et al., 2013). First, 10 mL of a homogeneous 10 mg/mL GO suspension was added to a beaker, and 0.1–0.4 g $MnCl_2$ and 0.2 g NaOH were added slowly to the suspension and stirred at 25 °C for 2 h. Then, the precipitate in the solution was collected by centrifugation and washed repeatedly with deionized water until pH was nearly neutral. After that, the precipitate was heated at 350 °C for 2 h in the air and the final product (in the form of black powder) was obtained. The as-synthesized samples were referred as 45-Mn_3O_4–rGO, 58-Mn_3O_4–rGO and 75-Mn_3O_4–rGO, on the basis of mass fraction of Mn_3O_4 in the Mn_3O_4–rGO nanocomposite. The product 75-Mn_3O_4–rGO (mass fraction of Mn_3O_4 was 75%) was used as the main Mn_3O_4–rGO nanocomposite in all the experiments, whereas 45-Mn_3O_4–rGO and 58-Mn_3O_4–rGO (containing 45% and 58% Mn_3O_4, respectively) were used in the reaction kinetics experiments to examine the effect of Mn_3O_4 loading on the reactivity of Mn_3O_4–rGO.

Two additional products resembling the Mn_3O_4 and rGO components of Mn_3O_4–rGO were also synthesized, each using the above mentioned procedures but without adding GO or $MnCl_2$ and NaOH, respectively. These two products are referred to as bare Mn_3O_4 and bare rGO hereafter. Additionally, to further understand the role of the rGO component in the reaction of 1-naphthylamine, a more completely reduced rGO was obtained by reducing bare rGO with N_2H_4. This product is referred to as rGO-N_2H_4. The detailed procedures used to synthesize these supplementary products are described in the Supplementary Data.

1-Naphthylamine (99.9%, Sigma–Aldrich, U.S.) was used as received. Stock solution of 1-naphthylamine was prepared in methanol and stored in the dark at −20 °C. Glass optical fibers coated with polyacrylate (PA fiber; thickness 35 μm; volume 15.4 μL/m) were purchased from Polymicro Technologies (U.S.).

2.2. Material characterization

The Mn_3O_4 content of the Mn_3O_4–rGO nanocomposites was analyzed by thermogravimetric analysis (NETZSCH STA 409PC, Germany) (Fig. S1). X-ray diffraction (XRD) analysis was performed using an X-ray diffractometer (Rigaku D/max-2500, Japan) (Fig. S2). Morphology and structures of the materials were examined using scanning electron microscopy (SEM) (Hitachi S-3500N, Japan) and transmission electron microscopy (TEM) (FEI, Tecnai G2 F20, U.S.) (Fig. S3). Surface chemistry properties of the materials before and after interacting with 1-naphthylamine were examined using X-ray photoelectron spectroscopy (XPS) (PHI 5000 Versa Probe, Japan) and Fourier transform infrared spectroscopy (FTIR) (Bruker TENSORTM 27, U.S.). Brunauer–Emmett–Teller (BET) surface area was determined using an accelerated surface area and porosimetry system (Micromeritics ASAP2010, U.S.).

The XRD pattern of 75-Mn_3O_4–rGO is very similar to that of bare Mn_3O_4, and correlates well with the hausmannite structure of Mn_3O_4 (JCPDS No. 89-4837). A weak broad peak around 2θ of 24–27° (the characteristic peak of rGO) was observed for 75-Mn_3O_4–rGO, whereas the peak at 2θ of 10.4° (the characteristic peak of GO) was not observed, indicating that GO was reduced during the synthesis (Pei and Cheng, 2012; Song et al., 2013). A similar weak broad peak was observed for bare rGO, confirming the reduction of GO during the synthesis, likely from heating. The SEM images (Fig. S3a and S3c) show that the Mn_3O_4 component of 75-Mn_3O_4–rGO and bare Mn_3O_4 had comparable morphology. The TEM images of 75-Mn_3O_4–rGO confirm that Mn_3O_4 particles (mostly 10–20 nm) were dispersed well on the rGO nanosheets

(Fig. S3d). This is consistent with the literature demonstrating that this synthesis approach results in Mn_3O_4 nanoparticles anchored to rGO nanosheets (Li et al., 2013; Nam et al., 2013). The BET surface area of 75-Mn_3O_4–rGO is 60.37 m^2/g, and that of bare Mn_3O_4 is 42.79 m^2/g. We were unable to measure the surface area of bare rGO because the powder flew away easily during the vacuuming process.

2.3. Batch reaction experiments

To initiate a reaction kinetic experiment, a certain amount of Mn_3O_4–rGO, bare Mn_3O_4 or bare rGO was added to a 250-mL amber glass vial and prewetted with deionized water for 24 h (when needed, pH was adjusted with NaOH or HCl). Afterward, a stock solution of 1-naphthylamine (in methanol, the volume percentage of methanol was kept below 0.1% (*v*/*v*) to minimize cosolvent effects) was added to the vial using a microsyringe to give a final 1-naphthylamine concentration of 5 mg/L, and the vial was filled with deionized water to leave minimal headspace. After that, the vial was sealed with a Teflon-lined screw cap and shaken with an orbital shaker at 25.0 ± 0.5 °C. At predetermined time intervals less than 0.6 mL aliquot was withdrawn to analyze the concentration of 1-naphthylamine. The aliquot was mixed with methanol (1:1, *v*:*v*), filtered through 0.22-μm membrane (Anpel Scientific Instrument, China), and analyzed with high-performance liquid chromatography (HPLC) (see below). At the end of the reaction kinetic experiment, a negligible depletion-solid-phase microextraction (nd-SPME) method was used to identify the transformation products of 1-naphthylamine (Wang et al., 2014). Briefly, a piece of glass fiber was added to the reaction vial and equilibrated for 3 d (the time required was determined in our previous study (Wang et al., 2014)). Then, the fiber was extracted with methanol, and the transformation products were analyzed with ultra-performance liquid chromatography–tandem quadrupole mass spectrometry (UPLC–MS/MS) (see below). Identification of all the reaction products was infeasible due to the lack of commercial standards. Thus, the most probable molecular structures of the reactive products were deduced based on the *m*/*z* values (Li and Lee, 1999; Li et al., 2003; Lin et al., 2009; Skarpeli-Liati et al., 2011).

A separate set of kinetic experiments was carried out using a slightly different experimental setup to examine the effect of dissolved O_2 on the reaction. Specifically, 40-mL amber glass vials equipped with gas-tight caps were used. This apparatus allowed controlling of O_2 concentration in the system by sparging with O_2 or purging with N_2; it also allowed sampling using a microsyringe without having to take off the cap. The reaction systems consisted of 60 mg/L Mn_3O_4–rGO or bare Mn_3O_4 and 30 mg/L 1-naphthylamine. After pre-wetting Mn_3O_4–rGO or bare Mn_3O_4, the aqueous suspension was purged with N_2 or sparged with O_2 for at least 2 h to achieve an O_2-deficit or O_2-rich environment. Then, the stock solution of 1-naphthylamine was added to initiate the reaction.

Another set of experiments was conducted to examine the oxidation of 1-naphthylamine in the presence of both Mn(II) and a rGO product. First, 12.5 mg of bare rGO or rGO-N_2H_4 was added to a 250-mL amber glass bottle containing deionized water, to give a concentration of 50 mg/L. After pre-wetting for 24 h, a stock solution of 1-naphthylamine was added to give a 1-naphthylamine concentration of 25 mg/L, and a stock solution of Mn(II) was added to give a total Mn(II) concentration of 1 mmol/L. The bottle was shaken with an orbital shaker at 25.0 ± 0.5 °C for 9 d. Next, the bottle was centrifuged at 3000 *g* for 20 min. Aliquots of the aqueous solution were withdrawn, mixed with methanol (1:1, *v*:*v*), filtered through 0.22-μm membrane filters, and analyzed with HPLC to determine the concentration of 1-naphthylamine. Oxidation of Mn(II) by bare rGO and rGO-N_2H_4 in these experiments was also examined, and the detailed procedures are given in Supplementary data.

2.4. Analytical methods

1-Naphthylamine was analyzed with a Waters 1100 HPLC equipped with a UV detector at 230 nm and a 4.6 × 150 mm SunFire-C18 column (Waters, U.S.). The mobile phase was acetonitrile–deionized water (60:40, *v*:*v*) at a flow rate of 1 mL/min. Transformation products of 1-naphthylamine were analyzed with a Waters UPLC–MS/MS equipped with an Acquity UPLC BEH C18 column (1.7 μm, 2.1 × 50 mm) (Xevo TQ-S, Waters, U.S.). The mobile-phase was methanol with a flow rate of 0.45 mL/min. The mass spectrometer was operated in the *m*/*z* 60–600 range for UPLC–MS/MS. The cone voltage was set to 40 V. The desolvation temperature and source temperature were 350 and 150 °C, respectively.

3. Results and discussion

3.1. Anchoring Mn_3O_4 to rGO enhanced its oxidation capacity

All three Mn_3O_4–rGO nanocomposites resulted in greater transformation of 1-naphthylamine than did bare Mn_3O_4 (Fig. 1). For example, nearly 75% 1-naphthylamine disappeared in the presence of 10 mg/L 75-Mn_3O_4–rGO, whereas the loss of 1-naphthylamine was only ~15% in the presence of 7.5 mg/L bare Mn_3O_4 (containing the same mass of Mn_3O_4 as in 75-Mn_3O_4–rGO). The observed pseudo first-order rate constant (k_{obs}) by 75-Mn_3O_4–rGO was 0.115 ± 0.007 d^{-1}, nearly one order of magnitude higher than that for bare Mn_3O_4 (0.0128 ± 0.0008 d^{-1}) (Table S1 and Fig. S4). Negligible loss of 1-naphthylamine was observed in the control experiment (aqueous 1-naphthylamine alone), indicating no significant photo transformation or biodegradation in the absence of Mn_3O_4–rGO or bare Mn_3O_4. Furthermore, only a 12% loss of 1-naphthylamine was observed in the presence of 2.5 mg/L bare rGO. Thus, it can be concluded that when

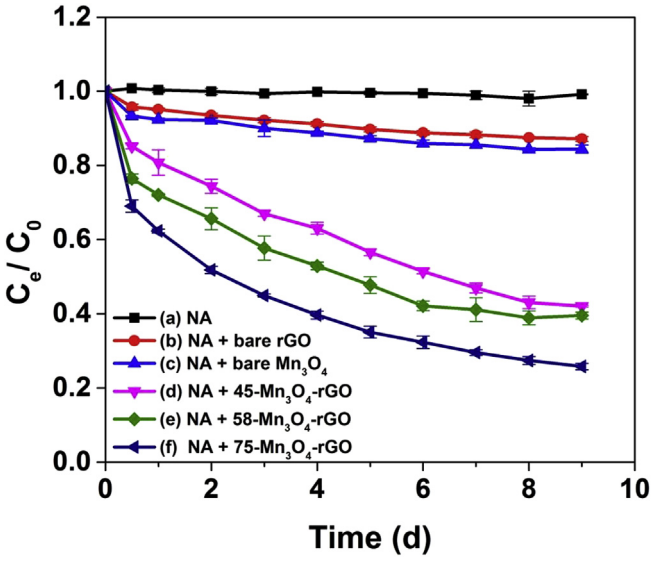

Fig. 1. Removal of 1-naphthylamine (NA, C_0 = 5 mg/L) in aqueous solutions: a) blank control (NA alone); b) with bare rGO; c) with bare Mn_3O_4; and d)–f) with Mn_3O_4–rGO. Reaction conditions: [bare Mn_3O_4] = 7.5 mg/L, [bare rGO] = 2.5 mg/L, [45-Mn_3O_4–rGO] = [58-Mn_3O_4–rGO] = [75-Mn_3O_4–rGO] = 10 mg/L. Error bars, in most cases smaller than the symbols, represent the range of duplicates.

Mn_3O_4 was anchored to rGO, a synergistic effect on the removal of 1-naphthylamine was achieved, as compared with the removal of 1-naphthylamine from the aqueous solution by bare Mn_3O_4 and bare rGO.

Multiple peaks were observed in the total ionic chromatogram of 1-naphthylamine and its reaction products by 75-Mn_3O_4–rGO and by bare Mn_3O_4 (Fig. S5). A series of products (mostly dimers of 1-naphthylamine) were identified on the basis of the *m/z* values (Fig. S6) (Li and Lee, 1999; Li et al., 2003). Previous studies have shown that the amino groups of aromatic amines are susceptible to chemical oxidation and can easily lose an electron; this results in the formation of amine radicals, which then form polymers through radical oxidative coupling reactions (Colón et al., 2002; Laha and Luthy, 1990; Li and Lee, 1999; Li et al., 2003; Schwarzenbach et al., 2003; Skarpeli-Liati et al., 2011). Interestingly, the species and distribution of oxidized products of 1-naphthylamine by 75-Mn_3O_4–rGO and by bare Mn_3O_4 were almost identical (Fig. S5), indicating that anchoring Mn_3O_4 to rGO did not change the reaction pathway through which Mn_3O_4 oxidizes 1-naphthylamine.

3.2. Changes in Mn_3O_4–rGO surface chemistry during oxidation of 1-naphthylamine

The XPS and FTIR data show collectively that the rGO component of 75-Mn_3O_4–rGO underwent further reduction during the transformation of 1-naphthylamine. The C 1s XPS spectrum of the as-prepared 75-Mn_3O_4–rGO (Fig. 2a and b) show four peaks that are associated with C–C/C=C (284.6 eV), C–O (286.7 eV), C=O (287.8 eV) and O–C=O (288.8 eV). After reacting with 1-naphthylamine, the width and intensity of the C–C/C=C peak increased, whereas the intensity of the C–O, C=O, and O–C=O peaks significantly decreased (Fig. 2b), indicating the reduction of the rGO component of 75-Mn_3O_4–rGO (Pei and Cheng, 2012). (Distributions of carbon species in 75-Mn_3O_4–rGO before and after the reaction with 1-naphthylamine are summarized in Table S2.) The FTIR spectra (Fig. 3) also show substantial decrease of O-functional groups (especially C–O) of 75-Mn_3O_4–rGO, upon reacting with 1-naphthylamine. Thus, on the basis of the combined spectroscopic evidence, it appears that the rGO component functioned as an oxidant in the transformation of 1-naphthylamine by 75-Mn_3O_4–rGO, and therefore, was reduced. This active participation of rGO in the reaction is distinctly different from the previously proposed roles of the GO/rGO support of metal oxide–graphene nanocomposites (i.e., enhancing dispersion of metal oxide, enhancing adsorption of contaminants, and conducting electrons) (Chandra et al., 2010; Fu et al., 2014; Leary and Westwood, 2011; Li et al., 2015; Lindfors et al., 2013; Shen et al., 2015; Upadhyay et al., 2014; Xu et al., 2015; Yao et al., 2013; Zhang et al., 2010). In comparison, both the XPS and FTIR spectra show that the distribution and abundance of surface O-functional groups of bare rGO did not change after interacting with 1-naphthylamine (Figs. S7 and S8).

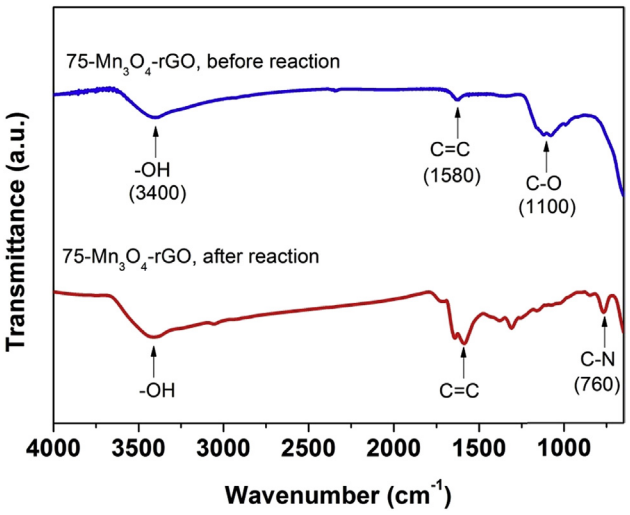

Fig. 3. FTIR spectra of 75-Mn_3O_4–rGO before and after reaction with 1-naphthylamine.

3.3. Role of rGO component of Mn_3O_4–rGO in mediating redox cycle of Mn(II)/Mn(III)

The rGO component of the Mn_3O_4–rGO nanocomposite may participate in the oxidation of 1-naphthyalmine by reacting directly with the organic molecules or by affecting the redox state of Mn_3O_4. The former was not very likely because the oxidation of 1-naphthylamine by Mn_3O_4 would take precedence, due to the higher oxidation potential of Mn_3O_4 than rGO (Chowdhury et al., 2009; Kauppila et al., 2014). The facts that bare rGO could not result in significant transformation of 1-naphthylamine and, in particular, that the surface chemistry of bare rGO remained unchanged upon interacting with 1-naphthylamine (Figs. S7 and S8) are consistent with this argument. Furthermore, whereas 75-Mn_3O_4–rGO exhibited significantly greater oxidation efficiency than did bare Mn_3O_4, the transformation pathways of 1-naphthylamine by 75-Mn_3O_4–rGO and by bare Mn_3O_4 were very

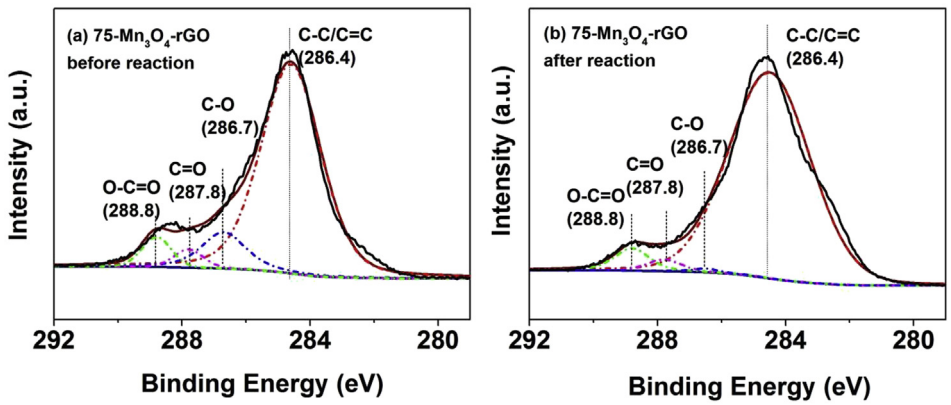

Fig. 2. XPS spectra of C 1s for 75-Mn_3O_4–rGO before and after reaction with 1-naphthylamine: a) 75-Mn_3O_4–rGO before reaction; and b) 75-Mn_3O_4–rGO after reaction.

similar (Fig. S5). This also indicates that the Mn_3O_4 component of Mn_3O_4–rGO was the primary oxidant. Thus, we postulate that the rGO component improved the oxidation efficiency of Mn_3O_4–rGO mainly by mediating the redox cycle of Mn, rather than reacting directly with 1-naphthylamine.

According to previous studies, the oxidation of 1-naphthylamine by MnO_x starts from the formation of a precursor complex between 1-naphthylamine and the surface of MnO_x, followed by a one-electron transfer within the complex, forming 1-naphthylamine radical species; the radical species then form oxidative products, accompanied with the reductive dissolution of Mn(II) (Li et al., 2003; Schwarzenbach et al., 2003; Skarpeli-Liati et al., 2011). For Mn_3O_4 the process can be expressed as:

$$\equiv Mn^{III} + NA \rightarrow (\equiv Mn^{III}, NA) \rightarrow (\equiv Mn^{II}, NA\cdot) \rightarrow Mn^{2+} + NA\cdot \quad (1)$$

$$NA\cdot \rightarrow \text{oxidative coupling products} \quad (2)$$

where NA denotes 1-naphthylamine, and the symbol "≡" indicates surface-associated species. When Mn_3O_4 is anchored to rGO, the surface Mn(II) species can be re-oxidized by rGO, and thus, regenerating surface Mn(III) species, which can then participate in the oxidation of 1-naphthylamine (i.e., Equation (1)). A pictorial illustration of the role of rGO is shown in Fig. 4. As shown in the XPS spectra (Fig. 2a) and FTIR spectra (Fig. 3), the rGO component of 75-Mn_3O_4–rGO contained considerable amounts of surface O-functional groups (epoxy and carbonyl moieties). These moieties can serve as the oxidants, and thus re-oxidize Mn(II) (Fan et al., 2010; Han et al., 2014; Li et al., 2013; Su and Loh, 2012). Oxidation of aqueous Mn^{2+} by rGO at room temperature has been reported (Han et al., 2014; Li et al., 2013). Furthermore, when bound to rGO the oxidative potential of Mn(II)/Mn(III) would be lowered, favoring the oxidation of Mn(II) to Mn(III). Such facilitated oxidation has previously been reported for metals bound to humic substances rich in carbonyl and carboxyl groups (Fulda et al., 2013; Latta et al., 2012; Vikesland and Valentine, 2002).

Re-oxidation of Mn(II) to Mn(III) by the rGO component of 75-Mn_3O_4–rGO is corroborated by the Mn 2p XPS spectra (Fig. S9). It has been proposed that the changes of peak position of Mn $2p_{3/2}$ indicate the changes of surface oxidation states of Mn (Chen et al., 2012b; Gorlin et al., 2014; Tseng et al., 2003). Specifically, the peak position at a higher binding energy implies a higher surface oxidation state of Mn in the solid samples. Fig. S9 shows that the peak position shifted toward lower binding energy after 75-Mn_3O_4–rGO or bare Mn_3O_4 reacted with 1-naphthylamine, which can be ascribed to a consumption of Mn(III) to form Mn(II) (Chen et al., 2012b; Gorlin et al., 2014). Because 75-Mn_3O_4–rGO resulted in much more significant oxidation of 1-naphthylamine than did bare Mn_3O_4 (Fig. 1), the peak shift to the lower binding energy should be more significant for 75-Mn_3O_4–rGO than for bare Mn_3O_4. However, this was not the case based on Fig. S9. The less than expected peak shift is consistent with the re-oxidation of Mn(II) to Mn(III) by the rGO component of 75-Mn_3O_4–rGO.

To further demonstrate that the rGO component of Mn_3O_4–rGO can facilitate the oxidation of 1-naphthylamine by regenerating an oxidant, Mn(III), we examined the transformation of 1-naphthylamine in systems containing Mn(II) and two different rGO forms—including bare rGO and rGO-N_2H_4—that represented different degrees of surface oxidation (see the FTIR results in Fig. S10). The hypothesis was that bare rGO would be able to oxidize the Mn(II) species bound to it and therefore, generate Mn(III), which would then oxidize 1-naphthylamine. In contrast, little or no enhanced removal of 1-naphthylamine would occur when the highly-reduced rGO-N_2H_4 was used, which would be much less effective in oxidizing Mn(II). The results (Fig. S11) clearly show that in the presence of bare rGO, the removal of 1-naphthylamine was more significant in the system containing Mn(II) than in the respective system in which Mn(II) was not added, whereas in the presence of rGO-N_2H_4 no such effect was observed. The total ionic chromatograms of 1-naphthylamine and its transformation products (Fig. S12) further show that adding Mn(II) significantly enhanced the transformation of 1-naphthylamine in the systems containing bare rGO (as indicated by the markedly increased peak intensity of reaction products), but not in the system containing rGO-N_2H_4. Moreover, the XPS Mn 2p spectra of bare rGO and rGO-N_2H_4 after interacting with Mn(II) (Fig. S13) show that more Mn(III) was formed on bare rGO than on rGO-N_2H_4, as evidenced by the higher binding energy of Mn $2p_{3/2}$ associated with bare rGO than with rGO-N_2H_4 (Chen et al., 2012b; Gorlin et al., 2014). Thus, the combined evidence in Fig. S10–S13 corroborates that the rGO component of Mn_3O_4–rGO is able to re-oxidize Mn(II) species to form oxidative Mn(III), which can then enhance the oxidation of 1-naphthylamine.

3.4. O_2 and pH effect experiments provide further evidence for rGO regenerating Mn(II)

To further demonstrate that it was rGO rather than other oxidants that facilitated the redox cycle of Mn(II)/Mn(III), additional experiments were conducted to understand the effects of O_2 on the oxidation of 1-naphthylamine by bare Mn_3O_4 and 75-Mn_3O_4–rGO (Fig. 5), in that oxidation of Mn(II) to Mn(III) can occur in aquatic environments in the presence of dissolved O_2 (Kessick and Morgan, 1975; Stauffer, 1986). Fig. 5 shows that sparging with O_2 slightly increased the kinetics of oxidative transformation of 1-naphthylamine by bare Mn_3O_4, whereas purging with N_2 inhibited reaction kinetics. However, the effect of O_2 in enhancing the oxidative efficiency of bare Mn_3O_4 was negligible compared with that of the rGO component of 75-Mn_3O_4–rGO. Interestingly, a much greater extent of 1-naphthylamine transformation was observed in the reaction regime of 75-Mn_3O_4–rGO with N_2-purging than in the regime of bare Mn_3O_4 with O_2-sparging (Fig. 5). Furthermore, sparging with O_2 did not substantially increase the rate of oxidative transformation of 1-naphthylamine by 75-Mn_3O_4–rGO. Thus, the rGO component of 75-Mn_3O_4–rGO was more effective in re-oxidizing Mn(II) than was dissolved O_2. This set of experiments also ruled out the possibility that the high oxidative efficiency of Mn_3O_4–rGO was due to a Fenton-like reaction (Watts

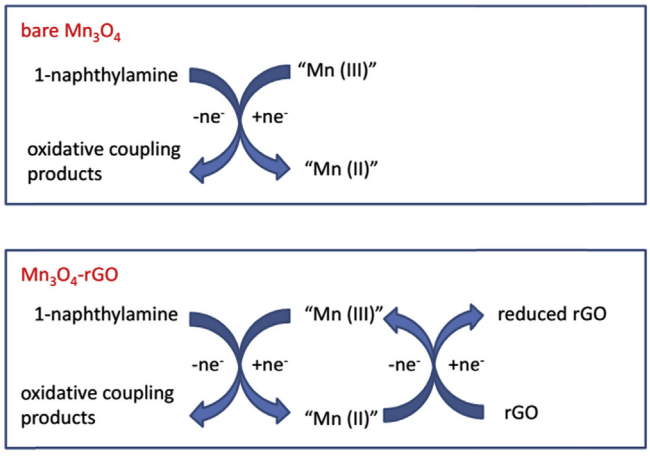

Fig. 4. Role of the rGO component of Mn_3O_4–rGO in mediating the redox cycle of Mn(II)/Mn(III) in the enhanced transformation of 1-naphthylamine by Mn_3O_4–rGO than by bare Mn_3O_4.

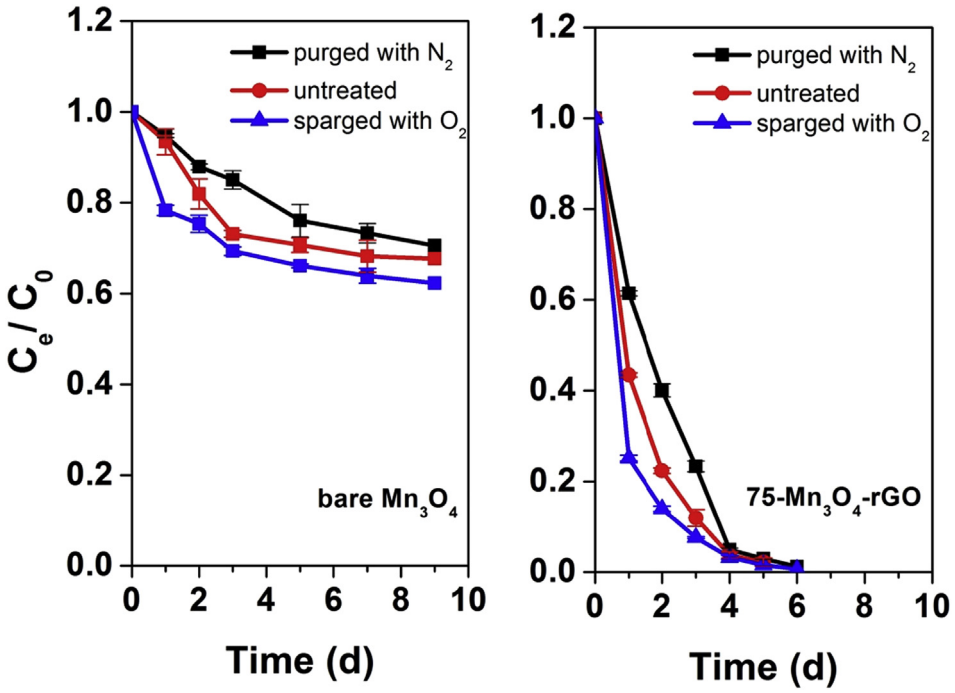

Fig. 5. Effects of O_2 on transformation of 1-naphthylamine (NA, $C_0 = 30$ mg/L) by bare Mn_3O_4 and 75-Mn_3O_4–rGO. The term "untreated" refers to experiments conducted without N_2 or O_2 treatment. Reaction conditions: [bare Mn_3O_4] = [75-Mn_3O_4–rGO] = 60 mg/L. Error bars represent the range of duplicates.

et al., 2005; Wuttig et al., 2013), i.e., O_2 was not activated by rGO to form a significant amount of highly oxidative hydroxyl radicals.

The role of rGO in mediating the redox cycle of Mn(II)/Mn(III) was also corroborated by the pH-dependent reactivity. Strikingly, completely opposite pH effects were observed between bare Mn_3O_4 and 75-Mn_3O_4–rGO (Fig. 6). Increasing pH significantly inhibited the oxidation of 1-naphthylamine by bare Mn_3O_4. This is attributed to the fact that increasing pH restrains the reduction of Mn_3O_4 to Mn^{2+},

$$Mn_3O_4(s) + 8H^+ + 2e^- \rightarrow 3Mn^{2+} + 3H_2O,\ E_0' = 1.824\ V \quad (3)$$

Nonetheless, increasing pH significantly enhanced the oxidation of 1-naphthylamine by 75-Mn_3O_4–rGO. This is consistent with the

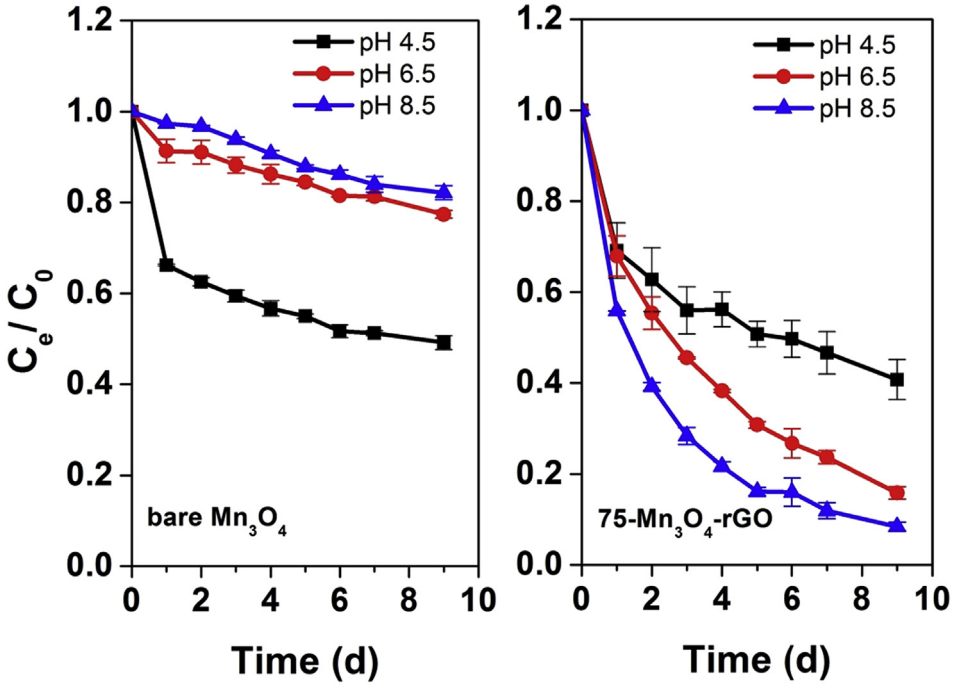

Fig. 6. Effects of pH on transformation of 1-naphthylamine (NA, $C_0 = 5$ mg/L) by bare Mn_3O_4 and 75-Mn_3O_4–rGO. Reaction conditions: [bare Mn_3O_4] = [75-Mn_3O_4–rGO] = 10 mg/L. Error bars represent the range of duplicates.

proposed role of rGO in re-oxidizing Mn(II). First, the deprotonation of the acidic O-functional groups of rGO at elevated pH could enhance the binding of Mn^{2+} to the surface of Mn_3O_4–rGO, which was beneficial for the re-oxidation of Mn(II) by rGO. Second, increasing pH could facilitate the oxidation of surface-bound Mn(II) to Mn(III) (Li et al., 2013),

$$rGO{\equiv}Mn^{II} + OH^- \rightarrow rGO^*{\equiv}Mn^{III} \quad (4)$$

where rGO^* denotes further reduced rGO after oxidizing Mn(II) to Mn(III). It has been proposed that oxidation of Mn(II) species bound to the surface of birnessite is enhanced at elevated pH (Lefkowitz et al., 2013), which supports the proposed reaction in Equation (4). Note that within the test pH range Mn_3O_4 should be positively charged (Shaughnessy et al., 2003). Thus, binding of Mn(II) to the surface groups of Mn_3O_4 (mainly in the form of $\equiv Mn^{III}OH_2^+$) (Stone, 1987; Stone and Morgan, 1984) and the subsequent re-oxidation was unlikely. Accordingly, in the reaction system containing bare Mn_3O_4 re-oxidation of Mn(II) at elevated pH should have been negligible. Moreover, pH had little effect on the removal of 1-naphthylamine by bare rGO (Fig. S14). This further corroborates that the significantly enhanced transformation of 1-naphthylamine by 75-Mn_3O_4–rGO at elevated pH was attributable to the enhanced efficiency of rGO in re-oxidizing Mn(II) with increasing pH.

4. Conclusions

Mn_3O_4–rGO nanocomposites exhibited much greater oxidation efficiency than bare Mn_3O_4. The rGO component improved the oxidation efficiency of Mn_3O_4 predominantly by re-oxidizing Mn(II) formed from the reaction between Mn_3O_4 and 1-naphthylamine, and thereby, regenerating surface-bound oxidative Mn(III) species (even though other mechanisms such as enhancing adsorption of contaminant cannot be ruled out). The discernment that the improved performance of Mn_3O_4–rGO nanocomposites over bare Mn_3O_4 is primarily due to re-oxidation of surface-associated Mn(II) to Mn(III) by rGO advances our mechanistic understanding of the interaction of graphene-based materials with anchored metal oxides. This finding may guide the development of superior metal oxide–graphene nanocomposites for contaminant removal.

Note that the synthesis of Mn_3O_4–rGO in this study involved heating, causing partial reduction of GO. Future studies can be directed to develop nanocomposites incorporating more oxidized forms of graphene substrates to further enhance the performance and stability of anchored metal oxides.

Acknowledgments

This project was supported by the Ministry of Science and Technology of China (Grant 2014CB932001), the National Natural Science Foundation of China (Grants 21237002 and 21425729), and Tianjin Municipal Science and Technology Commission (Grant 16JCYBJC22400). Partial funding was provided by the NSF ERC on Nanotechnology-Enabled Water Treatment (EEC-1449500).

Appendix A. Supplementary data

Supplementary data related to this article can be found at http://dx.doi.org/10.1016/j.watres.2016.07.023.

References

Appavoo, A.I., Hu, J., Huang, Y., Li, S.F.Y., Ong, S.L., 2014. Response surface modeling of Carbamazepine (CBZ) removal by Graphene-P25 nanocomposites/UVA process using central composite design. Water Res. 57, 270–279.

Chandra, V., Park, J., Chun, Y., Lee, J.W., Hwang, I.C., Kim, K.S., 2010. Water-dispersible magnetite-reduced graphene oxide composites for arsenic removal. ACS Nano 4 (7), 3979–3986.

Chang, H., Wu, H., 2013. Graphene-based nanocomposites: preparation, functionalization, and energy and environmental applications. Energy Environ. Sci. 6 (12), 3483–3507.

Chen, D., Feng, H., Li, J., 2012a. Graphene oxide: preparation, functionalization, and electrochemical applications. Chem. Rev. 112 (11), 6027–6053.

Chen, Z., Jiao, Z., Pan, D., Li, Z., Wu, M., Shek, C.H., Wu, C.M.L., Lai, J.K.L., 2012b. Recent advances in manganese oxide nanocrystals: fabrication, characterization, and microstructure. Chem. Rev. 112 (7), 3833–3855.

Chowdhury, A.N., Azam, M.S., Aktaruzzaman, M., Rahim, A., 2009. Oxidative and antibacterial activity of Mn_3O_4. J. Hazard. Mater. 172 (2–3), 1229–1235.

Colón, D., Weber, E.J., Baughman, G.L., 2002. Sediment-associated reactions of aromatic amines. 2. QSAR development. Environ. Sci. Technol. 36 (11), 2443–2450.

Dreyer, D.R., Jia, H.P., Bielawski, C.W., 2010. Graphene oxide: a convenient carbocatalyst for facilitating oxidation and hydration reactions. Angew. Chem. Int. Ed. 49 (38), 6813–6816.

Fan, Z.J., Kai, W., Yan, J., Wei, T., Zhi, L.J., Feng, J., Ren, Y.M., Song, L.-P., Wei, F., 2010. Facile synthesis of graphene nanosheets via Fe reduction of exfoliated graphite oxide. ACS Nano 5 (1), 191–198.

Fu, Y., Wang, J., Liu, Q., Zeng, H., 2014. Water-dispersible magnetic nanoparticle–graphene oxide composites for selenium removal. Carbon 77 (0), 710–721.

Fulda, B., Voegelin, A., Maurer, F., Christl, I., Kretzschmar, R., 2013. Copper redox transformation and complexation by reduced and oxidized soil humic acid. 1. X-ray absorption spectroscopy study. Environ. Sci. Technol. 47 (19), 10903–10911.

Georgakilas, V., Otyepka, M., Bourlinos, A.B., Chandra, V., Kim, N., Kemp, K.C., Hobza, P., Zboril, R., Kim, K.S., 2012. Functionalization of graphene: covalent and non-covalent approaches, derivatives and applications. Chem. Rev. 112 (11), 6156–6214.

Gorlin, Y., Lassalle-Kaiser, B., Benck, J.D., Gul, S., Webb, S.M., Yachandra, V.K., Yano, J., Jaramillo, T.F., 2014. In situ X-ray absorption spectroscopy investigation of a bifunctional manganese oxide catalyst with high activity for electrochemical water oxidation and oxygen reduction. J. Am. Chem. Soc. 135 (23), 8525–8534.

Gupta, V.K., Atar, N., Yola, M.L., Üstündağ, Z., Uzun, L., 2014. A novel magnetic Fe@Au core–shell nanoparticles anchored graphene oxide recyclable nanocatalyst for the reduction of nitrophenol compounds. Water Res. 48, 210–217.

Han, Z.J., Seo, D.H., Yick, S., Chen, J.H., Ostrikov, K., 2014. MnO_x/carbon nanotube/reduced graphene oxide nanohybrids as high-performance supercapacitor electrodes. NPG Asia Mater. 6, e140.

Jia, H.P., Dreyer, D.R., Bielawski, C.W., 2011. C–H oxidation using graphite oxide. Tetrahedron 67 (24), 4431–4434.

Kauppila, J., Lund, L., Laiho, T., Salomaki, M., Kankare, J., Lukkari, J., 2014. Effective low temperature reduction of graphene oxide with vanadium(III). J. Mater. Chem. C 2 (18), 3602–3609.

Kemp, K.C., Seema, H., Saleh, M., Le, N.H., Mahesh, K., Chandra, V., Kim, K.S., 2013. Environmental applications using graphene composites: water remediation and gas adsorption. Nanoscale 5 (8), 3149–3171.

Kessick, M.A., Morgan, J.J., 1975. Mechanism of autoxidation of manganese in aqueous solution. Environ. Sci. Technol. 9 (2), 157–159.

Krishnamoorthy, K., Veerapandian, M., Yun, K., Kim, S.J., 2013. The chemical and structural analysis of graphene oxide with different degrees of oxidation. Carbon 53 (0), 38–49.

Laha, S., Luthy, R.G., 1990. Oxidation of aniline and other primary aromatic amines by manganese dioxide. Environ. Sci. Technol. 24 (3), 363–373.

Latta, D.E., Bachman, J.E., Scherer, M.M., 2012. Fe electron transfer and atom exchange in goethite: influence of Al-substitution and anion sorption. Environ. Sci. Technol. 46 (19), 10614–10623.

Leary, R., Westwood, A., 2011. Carbonaceous nanomaterials for the enhancement of TiO_2 photocatalysis. Carbon 49 (3), 741–772.

Lefkowitz, J.P., Rouff, A.A., Elzinga, E.J., 2013. Influence of pH on the reductive transformation of birnessite by aqueous Mn(II). Environ. Sci. Technol. 47 (18), 10364–10371.

Li, H., Lee, L.S., 1999. Sorption and abiotic transformation of aniline and 1-naphthylamine by surface soils. Environ. Sci. Technol. 33 (11), 1864–1870.

Li, H., Lee, L.S., Schulze, D.G., Guest, C.A., 2003. Role of soil manganese in the oxidation of aromatic amines. Environ. Sci. Technol. 37 (12), 2686–2693.

Li, N., Geng, Z., Cao, M., Ren, L., Zhao, X., Liu, B., Tian, Y., Hu, C., 2013. Well-dispersed ultrafine Mn_3O_4 nanoparticles on graphene as a promising catalyst for the thermal decomposition of ammonium perchlorate. Carbon 54, 124–132.

Li, Y., Qu, J., Gao, F., Lv, S., Shi, L., He, C., Sun, J., 2015. In situ fabrication of Mn_3O_4 decorated graphene oxide as a synergistic catalyst for degradation of methylene blue. Appl. Catal. B Environ. 162, 268–274.

Lin, K., Liu, W., Gan, J., 2009. Oxidative removal of Bisphenol A by manganese dioxide: efficacy, products, and pathways. Environ. Sci. Technol. 43 (10), 3860–3864.

Lindfors, T., Österholm, A., Kauppila, J., Gyurcsányi, R.E., 2013. Enhanced electron transfer in composite films of reduced graphene oxide and poly(N-methylaniline). Carbon 63 (0), 588–592.

Liu, W., Ma, J., Shen, C., Wen, Y., Liu, W., 2016. A pH-responsive and magnetically separable dynamic system for efficient removal of highly dilute antibiotics in water. Water Res. 90, 24–33.

Lowry, G.V., Gregory, K.B., Apte, S.C., Lead, J.R., 2012. Transformations of

nanomaterials in the environment. Environ. Sci. Technol. 46 (13), 6893–6899.
Nam, I., Kim, N.D., Kim, G.P., Park, J., Yi, J., 2013. One step preparation of Mn_3O_4/graphene composites for use as an anode in Li ion batteries. J. Power Sources 244, 56–62.
Pastrana-Martínez, L.M., Morales-Torres, S., Figueiredo, J.L., Faria, J.L., Silva, A.M.T., 2015. Graphene oxide based ultrafiltration membranes for photocatalytic degradation of organic pollutants in salty water. Water Res. 77, 179–190.
Pei, S., Cheng, H.M., 2012. The reduction of graphene oxide. Carbon 50 (9), 3210–3228.
Pyun, J., 2011. Graphene oxide as catalyst: application of carbon materials beyond nanotechnology. Angew. Chem. Int. Ed. 50 (1), 46–48.
Schwarzenbach, R.P., Gschwend, P.M., Imboden, D., 2003. Environmental Organic Chemistry. Wiley-Inter-science, New York.
Shaughnessy, D.A., Nitsche, H., Booth, C.H., Shuh, D.K., Waychunas, G.A., Wilson, R.E., Gill, H., Cantrell, K.J., Serne, R.J., 2003. Molecular interfacial reactions between Pu(VI) and manganese oxide minerals manganite and hausmannite. Environ. Sci. Technol. 37 (15), 3367–3374.
Shen, Y., Fang, Q., Chen, B., 2015. Environmental applications of three-dimensional graphene-based macrostructures: adsorption, transformation, and detection. Environ. Sci. Technol. 49 (1), 67–84.
Skarpeli-Liati, M., Jiskra, M., Turgeon, A., Garr, A.N., Arnold, W.A., Cramer, C.J., Schwarzenbach, R.P., Hofstetter, T.B., 2011. Using nitrogen isotope fractionation to assess the oxidation of substituted anilines by manganese oxide. Environ. Sci. Technol. 45 (13), 5596–5604.
Song, L., Khoerunnisa, F., Gao, W., Dou, W., Hayashi, T., Kaneko, K., Endo, M., Ajayan, P.M., 2013. Effect of high-temperature thermal treatment on the structure and adsorption properties of reduced graphene oxide. Carbon 52 (0), 608–612.
Stauffer, R.E., 1986. Cycling of manganese and iron in Lake Mendota, Wisconsin. Environ. Sci. Technol. 20 (5), 449–457.
Stone, A.T., 1987. Reductive dissolution of manganese(III/IV) oxides by substituted phenols. Environ. Sci. Technol. 21 (10), 979–988.
Stone, A.T., Morgan, J.J., 1984. Reduction and dissolution of manganese(III) and manganese(IV) oxides by organics. 1. Reaction with hydroquinone. Environ. Sci. Technol. 18 (6), 450–456.
Su, C., Loh, K.P., 2012. Carbocatalysts: graphene oxide and its derivatives. Acc. Chem. Res. 46 (10), 2275–2285.
Sun, H., Liu, S., Zhou, G., Ang, H.M., Tad, M.O., Wang, S., 2012. Reduced graphene oxide for catalytic oxidation of aqueous organic pollutants. ACS Appl. Mater. Interfaces 4 (10), 5466–5471.
Tseng, T.K., Chu, H., Hsu, H.H., 2003. Characterization of α-Alumina-supported manganese oxide as an incineration catalyst for trichloroethylene. Environ. Sci. Technol. 37 (1), 171–176.
Upadhyay, R.K., Soin, N., Roy, S.S., 2014. Role of graphene/metal oxide composites as photocatalysts, adsorbents and disinfectants in water treatment: a review. RSC Adv. 4 (8), 3823–3851.
Vikesland, P.J., Valentine, R.L., 2002. Iron oxide surface-catalyzed oxidation of ferrous iron by monochloramine: implications of oxide type and carbonate on reactivity. Environ. Sci. Technol. 36 (3), 512–519.
Wan, X., Huang, Y., Chen, Y., 2012. Focusing on energy and optoelectronic applications: a journey for graphene and graphene oxide at large scale. Acc. Chem. Res. 45 (4), 598–607.
Wang, F., Haftka, J.J.H., Sinnige, T.L., Hermens, J.L.M., Chen, W., 2014. Adsorption of polar, nonpolar, and substituted aromatics to colloidal graphene oxide nanoparticles. Environ. Pollut. 186, 226–233.
Wang, G., Feng, W., Zeng, X., Wang, Z., Feng, C., McCarthy, D.T., Deletic, A., Zhang, X., 2016. Highly recoverable TiO_2–GO nanocomposites for stormwater disinfection. Water Res. 94, 363–370.
Watts, R.J., Sarasa, J., Loge, F.J., Teel, A.L., 2005. Oxidative and reductive pathways in manganese-catalyzed Fenton's reactions. J. Environ. Eng. 131 (1), 158–164.
Wuttig, K., Heller, M.I., Croot, P.L., 2013. Reactivity of inorganic Mn and Mn desferrioxamine B with O_2, O_2^-, and H_2O_2 in seawater. Environ. Sci. Technol. 47 (18), 10257–10265.
Xu, H., Qu, Z., Zong, C., Huang, W., Quan, F., Yan, N., 2015. MnO_x/Graphene for the catalytic oxidation and adsorption of elemental mercury. Environ. Sci. Technol. 49 (11), 6823–6830.
Yao, Y., Xu, C., Yu, S., Zhang, D., Wang, S., 2013. Facile synthesis of Mn_3O_4-reduced graphene oxide hybrids for catalytic decomposition of aqueous organics. Industrial Eng. Chem. Res. 52, 3637–3645.
Zhang, X., Yang, Y., Guo, S., Hu, F., Liu, L., 2015. Mesoporous $Ni_{0.85}Se$ nanospheres grown in situ on graphene with high performance in dye-sensitized solar cells. ACS Appl. Mater. Interfaces 7 (16), 8457–8464.
Zhang, Y., Tang, Z.-R., Fu, X., Xu, Y.J., 2010. TiO_2–Graphene nanocomposites for gas-phase photocatalytic degradation of volatile aromatic pollutant: is TiO_2–-graphene truly different from other TiO_2–carbon composite materials? ACS Nano 4 (12), 7303–7314.